Eur. Phys. J. B **46**, 355–361 (2005)
DOI: 10.1140/epjb/e2005-00255-7

THE EUROPEAN PHYSICAL JOURNAL B

Charge transport mechanism of vanadium pentoxide xerogel-polyaniline nanocomposite

S. De, A. Dey, and S.K. De[a]

Department of Materials Science, Indian Association for the Cultivation of Science, Jadavpur, Kolkata 700 032, India

Received 9 September 2004 / Received in final form 25 May 2005
Published online 18 August 2005 –

Abstract. The nanocomposites of conducting polyaniline are prepared by intercalating into the layers of vanadium pentoxide (V_2O_5) xerogel. The intercalation is confirmed by the observation of lattice expansion of V_2O_5 xerogel. Dc conductivity of the gel follows Arrhenius type temperature dependence while the nanocomposites exhibit three dimensional variable range hopping. The ac conductivity and dielectric properties are extensively studied at low temperature up to the frequency of 10 MHz. Two semicircles in Cole-Cole plot of impedance are found for the nanocomposites. The ac conductivity spectra reveal three frequency regions. The frequency exponent in the lower frequency region is nearer to 2. The dielectric response exhibit broad spectra which are analyzed by Cole-Cole distribution function. The peak frequency of dielectric spectra appears at the first cross over frequency of conductivity spectra.

PACS. 71.20.Tx Fullerenes and related materials; intercalation compounds – 73.63.-b Electronic transport in nanoscale materials and structures – 72.80.Le Polymers; organic compounds (including organic semiconductors) – 77.22.Gm Dielectric loss and relaxation

1 Introduction

The synthesis of conducting polymers (CP) by encapsulating into inorganic materials is a fascinating field in nanomaterials [1,2]. The incorporation is usually done in mesoporous, microporous, crystalline and amorphous solids, which are used as host materials for the conducting polymers. The encapsulation protects CP from atmosphere and also chemical attack. The most advantageous is that it eliminates interchain interactions of polymers. This enables to study the electronic properties and charge transport mechanisms of an isolated polymer chain. The addressing of individual chain leads to potential applications in molecular electronics. The incorporation of polymer is generally done by two ways: one is insertion of preformed polymer in the host and the other is polymerization within the layers of host.

Intercalative polymerization of conducting polymers inside the layered structures needs substantial oxidizing power. Among layered materials namely, FeOCl [3,4], V_2O_5 [5,6] and α-$RuCl_3$ [7] are suitable for the post-intercalation polymerization. Crystalline vanadium pentoxide has sufficiently strong oxidizing power among the high oxidation transition metal oxides. The intercalation of small ions are only possible due to strong interlayer bonding interactions. The vanadium pentoxide xerogel as represented by $V_2O_5.nH_2O$ are layered materials with water in the interlayer space [8]. The distance between two layers depend on the amount of intercalated water. Water molecule is very weakly hydrogen bonded to the oxide network. Vanadium pentoxide xerogel with higher interlayer distance is suitable for intercalation of a variety of guest specimen. The intercalation of polyanilie (PANI) [5], polypyrrole (PPY), polyethylene oxide (PEO) [9,10], poly ethylene dioxythiophene (PEDOT) [11] in V_2O_5 have been performed. Redox intercalation modifies the electronic structure of host material V_2O_5 both by expanding the interlayer distance and changing the electronic configuration of V^{5+} ions. During the polymerization process V^{5+} transfers to V^{4+} which yields mixed valence behavior of V atoms. Xerogels are also proton conductors which mainly depend on the amount of water. The nanocomposites consist of both electronic and protonic conductors. The exact transport mechanism of such mixed electronic-protonic conduction still remains unclear.

The understanding of charge transport mechanism in composite materials is important both from fundamental and technological point of view. The impedance measurement is one of the powerful techniques to characterize and realize the charge transport process in the complex materials. In the composites, the interface between different constituents creates further complication in determining the nature of charge transport. Impedance spectroscopy allows to distinguish the contributions of bulk and interface effects. In the present paper we describe the conduction mechanism and dielectric properties by measurement of ac impedance.

[a] e-mail: msskd@mahendra.iacs.res.in

2 Experimental

Preparation of $V_2O_5.nH_2O$ Xerogel

The preparation of $V_2O_5.nH_2O$ xerogel has been followed as described by Lemerle et al. [12]. In a typical synthesis, 2 gm of sodium metavanadate is dissolved in 125 ml of deionized water. The resulting solution is passed through a H^+ ion exchanger column, packed with 15 gm of resin (Dowex-50X2, 200-400) forming a pale orange solution of HVO_3. Aqueous HVO_3 solution is then dried in air at room temperature, which is polymerized to a red V_2O_5 xerogel (sample S1) within few days. After evaporation of excess water dark red film is formed and it is grounded to powder for subsequent use.

Preparation of $(PANI)_xV_2O_5.nH_2O$

Two different composites (sample S2 and S3) are prepared with different amount of aniline and $V_2O_5.nH_2O$ xerogel. 0.5 ml and 1 ml aniline are dispersed in 20 ml deionized water for sample S2 and S3 respectively, followed by addition of 0.5 gm of V_2O_5 xerogel in each case. The mixture is allowed to stand at room temperature for 5 h in air. The product is isolated by centrifugation, washed with acetone and dried in vacuum at room temperature. Green powder obtained is then pressed to form pellet and used for characterizations and transport measurements.

The X-ray powder diffraction studies are carried out with Philips Diffractometer (PW 1710) in the range 2−40° using Cu-K_α radiation. Fourier transform infrared (FTIR) spectra are recorded from pressed KBr pellets using a Perkin-Elmer-1600 FTIR spectrometer. Elemental analysis for weight percentage measurements is done using Perkin Elmer-2400 Series-II CHN analyzer.

The ac conductivity as a function of frequency is measured by 4192A Agilent Impedance Analyzer upto the frequency of 10 MHz at different temperatures. The electrical contacts are made by silver paint. The complex dielectric constants are obtained from the measurements of capacitance (C) and dissipation factor (D). The real part of dielectric constant ϵ_1 is evaluated from the relation $C = \epsilon_1\epsilon_0 a/t$, where ϵ_0 is the vacuum permittivity, a is the area and t is the thickness of the sample. The imaginary component is calculated from the dissipation factor, $\epsilon_2 = D\epsilon_1$. The ac conductivity $\sigma(\omega) = \omega\epsilon_2(\omega)$ is investigated at various temperatures. The complex impedance, Z is determined from the complex dielectric function ϵ, $Z = t/j\omega a\epsilon$

3 Results and discussion

The water content and the composition of material $(PANI)_xV_2O_5.nH_2O$ are determined by the elemental carbon, hydrogen and nitrogen (CHN) analyzer. The percentages of C, H, N and the values of x and n for different samples are shown in Table 1. The actual C/N = 6 ratio in PANI (-C_6H_4NH-) is almost maintained in all the composites. The amount of intercalated water in xerogel is 1.97 and it decreases with intercalation of polyaniline (PANI). This indicates that PANI is formed within the layers of gel through the replacement of water.

Table 1. Chemical compositions of $(C_6H_5N)_x$ $V_2O_5.nH_2O$ and value of x and n, calculated from CHN data.

Sample	C(%)	H(%)	N(%)	x	n
S1	-	1.83	-	-	1.97
S2	19.03	1.42	3.12	0.64	0.11
S3	22.01	1.59	4.09	0.77	0.06

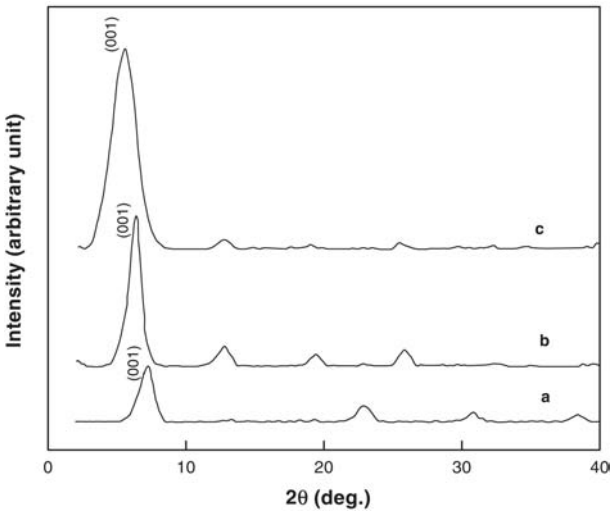

Fig. 1. X-ray diffraction pattern of (a) $V_2O_5.1.97H_2O$, (b) $(PANI)_{0.64}V_2O_5.0.11H_2O$ (c) $(PANI)_{0.77}V_2O_5.0.06H_2O$.

The X-ray diffraction (XRD) patterns of $V_2O_5.nH_2O$ and the composites are shown in Figure 1. The first peak in Figure 1a indicates (00l) reflections. The interlayer distance in the (00l) direction is estimated from Bragg's law, $2d\sin\theta = \lambda$. The layer spacing of gel with 1.97 H_2O is 12.10 Å. The first peak in Figure 1b shifts to lower angle which corresponds to the lattice expansion from 12.10 Å to 13.87 Å due to the intercalation of PANI. The maximum lattice expansion for $x = 0.77$ is 3.72 Å. The intercalation of PANI occurs through removal of water layer which is about 2.8 Å. The real lateral size of PANI molecule is around 5 Å.

The FTIR spectra of the gel and the nanocomposites are shown in Figure 2. The absorptions at 764 and 517 cm^{-1} are for V-O-V stretching modes and 1010 cm^{-1} is for V=O stretching. The spectra of the nanocomposites reveal the bands 1000−508 cm^{-1} corresponding to V_2O_5 and 1600−1100 cm^{-1} characteristic of PANI. The bands 1590, 1487 cm^{-1} originate from C-C ring stretching and 1307 cm^{-1} from C-H bending or C-N stretching of PANI. The identical XRD and FTIR spectra except the small changes in the peaks indicate the existence of layered structure of $V_2O_5.nH_2O$ after intercalation.

The room temperature dc conductivity $\sigma_{dc}(RT)$ of the gel is 5.08×10^{-6} S/cm and that of sample S3 is 1.97×10^{-3} S/cm. Intercalation of PANI into gel enhances the conductivity by about 1000 times through out the composition range. The increase of conductivity with

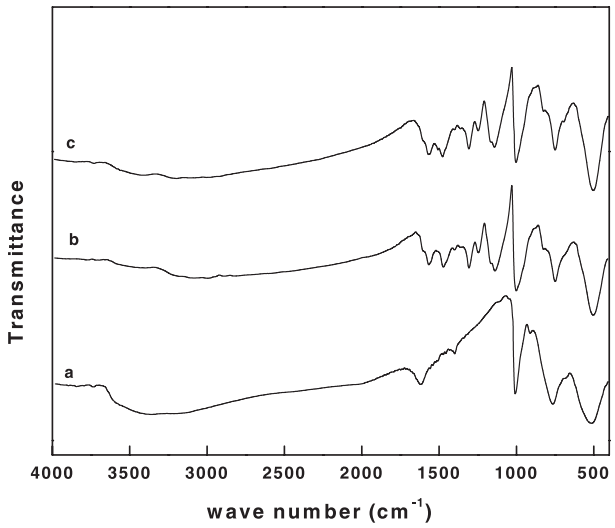

Fig. 2. Fourier Transform Infrared (FTIR) spectra of (a) $V_2O_5.1.97H_2O$, (b) $(PANI)_{0.64}V_2O_5.0.11H_2O$ (c) $(PANI)_{0.77}V_2O_5.0.06H_2O$.

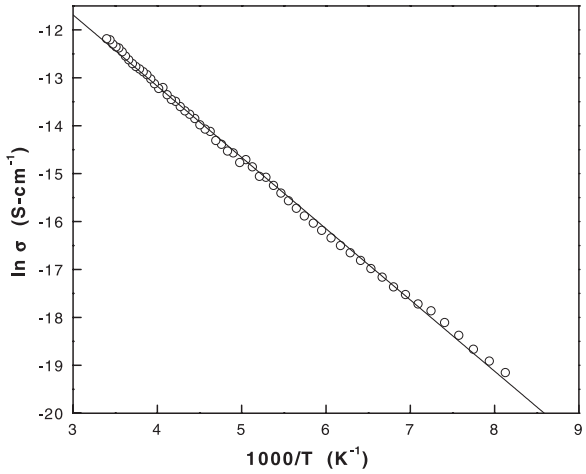

Fig. 3. Temperature variation of dc conductivity of V_2O_5 xerogel.

PANI concentration is due to the formation of more conducting PANI in the network of oxide gel and the increase of polymer chain length. The temperature dependence of $\ln \sigma_{dc}(T)$ of sample S1 is shown in Figure 3. The straight line of $\ln \sigma_{dc}(T)$ vs. $1/T$ suggests that thermally activated conduction process occurs. Thus the conductivity as a function of temperature can be represented by the relation,

$$\sigma(T) = \sigma_a \exp(-(E/kT)) \quad (1)$$

where E is the activation energy and k is the Boltzmann constant. The estimated value of E is 0.13 eV.

The variation of dc conductivity with temperature for the nanocomposites (S2 and S3) are shown in Figure 4. The linear behavior of $\ln \sigma_{dc}(T)$ with $T^{-1/4}$ indicates that $\sigma_{dc}(T)$ follows three dimensional variable range hopping (VRH) model [13],

$$\sigma(T) = \sigma_0 \exp(-(T_0/T)^{1/4}). \quad (2)$$

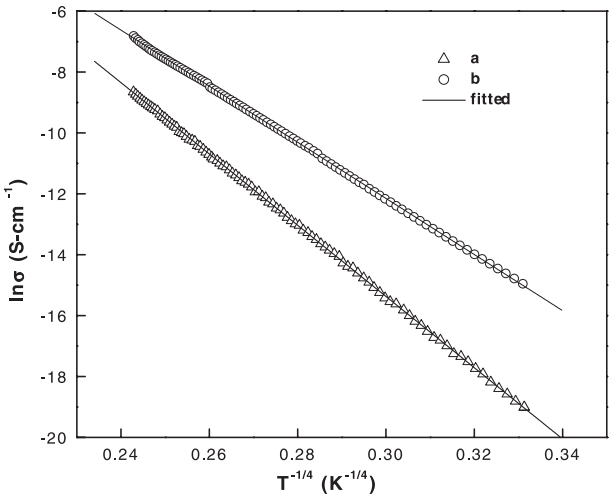

Fig. 4. Variable-temperature dc conductivity for two nanocomposites (a) $(PANI)_{0.64}V_2O_5.0.11H_2O$ (b) $(PANI)_{0.77}V_2O_5.0.06H_2O$.

The characteristic temperature $T_0 = 16/(kL^3N(E_F))$, where L is the localization length and $N(E_F)$ is the density of states at the Fermi level. The slopes of straight lines in Figure 4 give the values of $T_0 = 18.74 \times 10^7$ K of S2 and 7.20×10^7 K of S3. The smaller value of T_0 i.e. the larger of L suggests that sample S3 is more conductive than that of S2.

The incorporation of PANI into V_2O_5 induces V^{4+} ions during redox reaction. The formation of V^{4+} with d^1 conduction electrons gives semiconducting behavior. Electric conduction in the oxide network is due to hopping of electrons from V^{4+} sites to V^{5+}. Electrical conduction in PANI arises from the delocalized π electrons along the backbone of polymer. The intercalated PANI leads to two different types of conduction processes. Pure gel reveals thermally activated type conduction while the nanocomposites show VRH type conduction. Thus confined PANI in the nanocomposites plays an important factor in dc conduction process. Electrons are responsible for dc conduction in the nanocomposites.

The real part of frequency dispersion of conductivity $\sigma(\omega)$ at various temperatures have been investigated. The ac conductivity for sample S3 at different temperatures are shown in Figure 5. The $\sigma(\omega)$ starts to increase from the lowest frequency for gel. The samples S2 and S3 exhibit plateau region at lower frequency and then starts to increase at some onset frequency, ω_0 which decreases with lowering of temperature. The difference in the characteristic spectrum of $\sigma(\omega)$ is mainly due to the change of dc conductivity with concentration of PANI and temperature. The ac spectra exhibit three distinct frequency regimes depending on temperature. The low frequency region (I) shows strong frequency dispersion of conductivity. The intermediate (II) and high frequency domains (III) have comparatively weaker frequency dependency. The domain III is only observed at low temperature and high frequency. The distinct three regions of $\sigma(\omega)$ for sample S3 are shown in Figure 6.

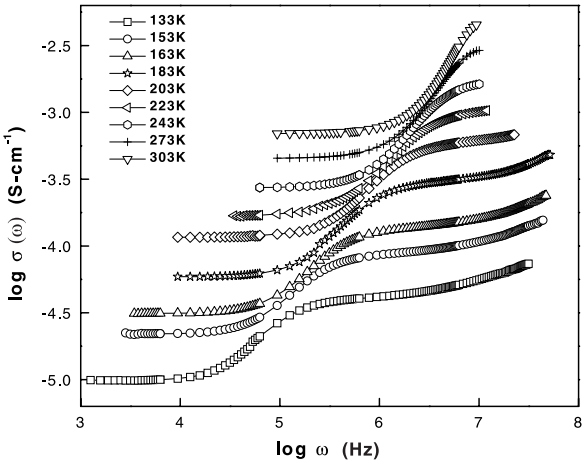

Fig. 5. Frequency dependence of conductivity at different temperatures of $(PANI)_{0.77}V_2O_5.0.06H_2O$.

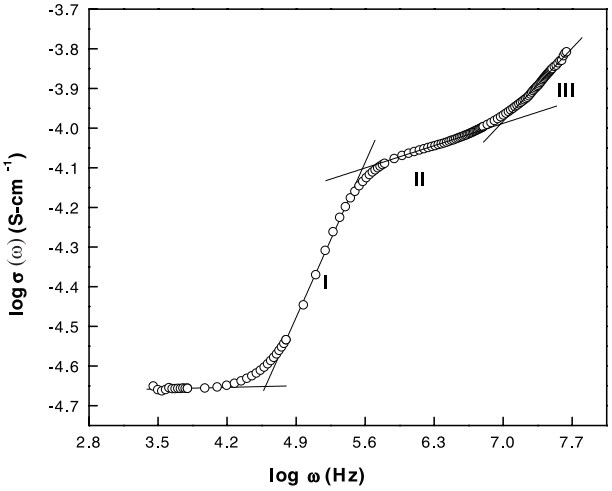

Fig. 6. Three distinct regions of ac conductivity for $(PANI)_{0.77}V_2O_5.0.06H_2O$ at 153 K.

Table 2. Activation energies E_0, E_{c_1} and E_{c_2} corresponding onset and crossover frequencies.

Sample	E_0(meV)	E_{c_1}(meV)	E_{c_2}(meV)
S1	-	353	247
S2	10.6	85.5	74.3
S3	10.4	90.9	60.5

The onset frequency ω_0 is calculated from the intersection of dc line with the extrapolated constant ac line. The other two cross over frequencies ω_{c1} and ω_{c2} at various temperatures are also evaluated in the similar way as shown in Figure 6. The temperature dependence of onset frequency and cross over frequencies exhibit Arrhenius type behavior and the activation energies are shown in Table 2. The activation energies of the nanocomposites are smaller by about one order of magnitude.

The conductivity as a function of frequency for disordered solids, ionic glasses [14,15] and polymers [16] is well described by the power law of frequency, $\sigma(\omega) \propto \omega^s$,

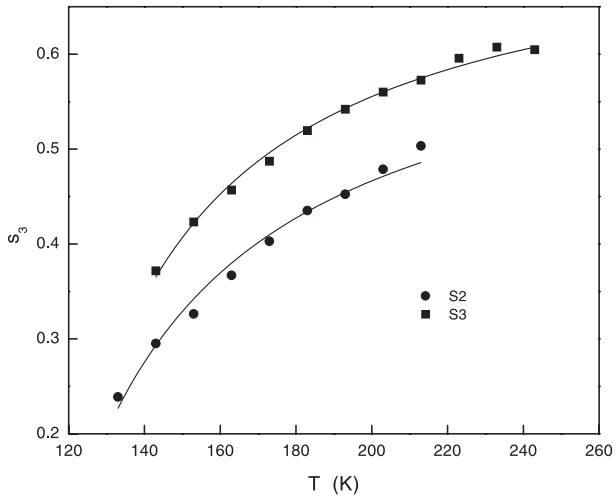

Fig. 7. Temperature variation of frequency exponent s_3 of two nanocomposites.

s lies between 0 and 1. The total conductivity at a given temperature is analyzed by the relation,

$$\sigma(\omega) = \sigma_{dc} + A_1\omega^{s_1} + A_2\omega^{s_2} + A_3\omega^{s_3} \qquad (3)$$

where σ_{dc} is dc conductivity, A's are dependent on temperature and s is the frequency exponent. The second, third and fourth terms in equation (3) represent three frequency domains. The exponent s at different temperatures for each frequency domain is evaluated by fitting equation (3). The exponent s in the region I lies between 1.5 and 2 and are almost independent of temperature. In other two regions it is between 0.1 and 0.6.

The high frequency impedance spectra give rise to bulk effect which is described later. Charge conduction process can be obtained from the temperature dependence of high frequency exponent s_3 as shown in Figure 7. In the pair approximation, frequency dependent conductivity is usually described by tunnelling and hopping of conduction electrons. Increase of s_3 with temperature suggests small polaron tunnelling which can be expressed as [15]

$$s_3 = 1 - \frac{4}{\ln(\frac{1}{\omega\tau_0}) - \frac{W_H}{kT}} \qquad (4)$$

where τ_0 is inverse phonon frequency, W_H is activation energy for polaron transfer. A reasonable good fitting with the experimental result confirms that small polaron tunnelling conduction process occurs in the intercalated systems. The calculated activation energies are 80 meV and 117 meV for nanocomposites S2 and S3 respectively.

The universal dynamic response and the limiting value of $s = 1$ is found in many materials. The frequency dispersion curve up to some MHz can be represented by a single frequency exponent. More than one power law dispersions are only observed in a very few class of materials such as alkali glasses [17] and carbon black-polymer composites [18]. Temperature induces two power law dispersions for alkali glasses. In case of carbon black-polymer nanocomposites, two successive frequency regimes are

found in THz region. Maass et al. [19] by Monte Carlo simulation with Coulomb interaction predicted that the exponent increases to unity with lowering of temperature. The regions I and II arise from the diffusive motion of charge carriers and region III is due to correlated local motion of dipolar reorientation. Recently, the different frequency regions are theoretically interpreted by relaxation mode theory [20]. The lower frequency regions are attributed to the extended nondiffusing and the higher frequency regions are localized nondiffusing mode. Based on this theory, Ishii et al. [21] showed that the exponent is greater than 1 and tends to attain 2 with increasing temperature in region I and it is less than 1 in other two regions. The theoretical cross over frequencies are thermally activated. The present experimental results are consistent with this theory.

The bulk and interface has different polarization properties. The plot of real part (Z_1) vs. imaginary part (Z_2) of complex impedance (Z) known as Cole-Cole plot are used to separate bulk and interface phenomena. In case of V_2O_5 xerogel, Cole-Cole plot show a straight line almost parallel to imaginary axis at room temperature due to low conductivity. The same plot exhibits semicircle and straight line at an intermediate temperature 193 K. In other temperatures below and above 193 K only one incomplete arc is obtained. The incomplete arc instead of a perfect semicircle is observed due to the limitation of measurements in frequency and impedance of the equipment. Each semicircle in Cole-Cole plot corresponds to a particular relaxation process. The relaxation mechanism of the material can be represented by the parallel combination of real resistor and capacitor. The diameter of the semicircle gives the resistance and the capacitance can be determined from the peak frequency of the semicircle. The different diameters of two semicircles at low and high frequencies indicate the presence of two regions containing high and low resistances. The resistance of the bulk is smaller than the interface. As the thickness of the interface is very small, capacitance will be very large compared to the bulk. Thus the two semicircles are due to the charge transport within the bulk and the interface. For sample S2, only one semicircle is found in the temperature interval of 295−215 K. The appearance of second semicircle below 200 K at low frequency implies the significant effect of interface. The bulk and interface effects are contributing at temperatures 303−133 K which are evident from the presence of two semicircles for sample S3 as shown in Figure 8. The frequency which separates between bulk and interface effects shifts to lower values with decreasing temperature. The insertion of PANI diminishes the resistance and capacitance of the interface.

The real part of the dielectric constant (ϵ_1) for the gel is about 10^4 at the lowest measured frequency which depends on temperature. The frequency independent behavior at the lowest frequencies indicate that electrode polarization effect is absent. The ϵ_1 decreases sharply with increasing frequency after some frequency which shifts to lower frequency with decreasing temperature. The intercalation of PANI reduces the magnitude of ϵ_1 which

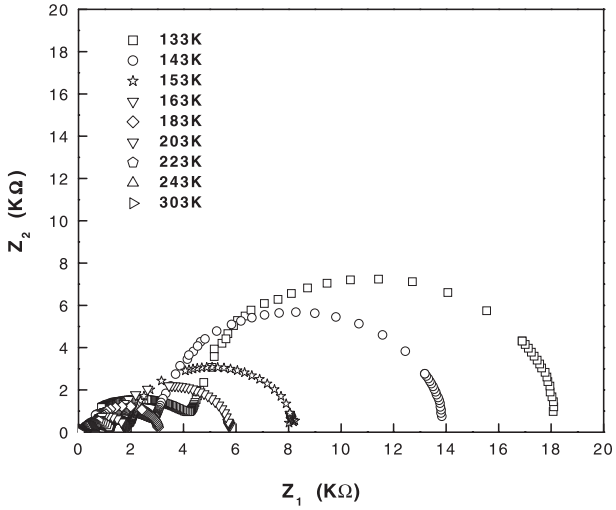

Fig. 8. Complex impedance plot(Cole-Cole plot) for $(PANI)_{0.77}V_2O_5.0.06H_2O$ at different temperatures.

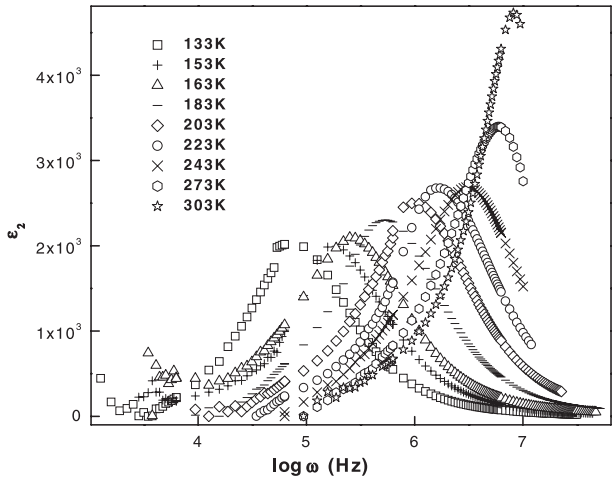

Fig. 9. Frequency dependence of imaginary part of dielectric constant at different temperatures of $(PANI)_{0.77}V_2O_5.0.06H_2O$.

indicates that water molecule contributes largely to the gel for greater value of ϵ_1.

The imaginary component of the dielectric constants at different temperatures for sample S3 is shown in Figure 9. The peak position moves to lower frequency with lowering of temperature. Dielectric relaxation of water [22] is in the range of GHz. Thus the peak is not due to dielectric relaxation of polar water molecule. The experimental data are best fitted by Cole-Cole complex dielectric function [23] as given by

$$\epsilon^* = \epsilon_\infty + \frac{\epsilon_s - \epsilon_\infty}{1 + (i\omega\tau)^{1-\alpha}} \tag{5}$$

where ϵ_∞ is the high frequency permittivity, ϵ_s is the static permittivity and τ is the average relaxation time which is given at the frequency of maximum dielectric loss. The difference $\Delta\epsilon = \epsilon_s - \epsilon_\infty$ is known as the dielectric relaxation strength. The parameter α describes the distribution of

Table 3. Dielectric strength ($\Delta\epsilon$) and Cole-Cole best-fit parameters τ and α for dielectric loss spectra of sample S3.

Temperature (K)	$\Delta\epsilon$	$\tau \times 10^6$(s)	α
133	4792.01	4.26	0.070
143	4993.32	3.16	0.081
153	5036.76	1.88	0.117
163	5175.79	1.56	0.127
173	5214.66	0.99	0.089
183	5560.84	0.79	0.099
193	5900.51	0.52	0.123
203	5560.84	0.34	0.099

the relaxation time of the system. Debye relaxation is obtained for $\alpha = 0$. The deviation of α from 0 indicates the broad distribution of relaxation time in the spectrum. The best fitted parameters are shown in Table 3. The values of α are different from zero which indicate the deviation from ideal Debye relaxation process. Much broader dielectric loss peaks are found at all temperatures for sample S1. The intercalation of PANI reduces the width of loss peak.

The dielectric loss spectra show well defined peak at different temperatures. The appearance of peak is well described by empirical Cole-Cole function. The high frequency ($\omega\tau \gg 1$) tails of dielectric loss spectra are found to decay as a power of frequency $\omega^{\alpha-1}$. Thus the exponent α in equation (5) can be related to the frequency exponent s in equation (3) in the high frequency region only. The parameter α is connected with the continuous distribution of relaxation times around the value τ. The estimated α represents the peak in the entire frequency region. Hence the values of α can not be compared with frequency exponent s.

The mean relaxation time τ for a particular temperature is calculated from the fits to equation (5). The calculated relaxation rate as a function of temperature is depicted in Figure 10. Straight line curves indicate Arrhenius type behavior in dielectric relaxation time. The activation energies as calculated from the slopes of straight lines are 352, 97 and 95 meV for S1, S2 and S3 respectively. The most interesting fact is that these values are almost equivalent to that of the first crossover frequency as shown in Table 2.

In the xerogel water molecules are intercalated in lamellar space of oxide. The molecular interaction between H_2O and oxide layers leads to the formation of hydroxyl group (OH). Dissociation of H_2O occurs due to the high ionic potential of V^{+5} ion which produces acidic H_3O^+ ions [24,25]. Ionic conduction arises from proton diffusion through gel matrix and it is strongly related to the number of water molecules. Aniline monomer is intercalated within the galleries of gels with removal of water molecule and concomitantly polymerized into PANI through proton exchange reactions. Intercalation reduces the number of water molecule as shown in Table 1 and consequently proton concentration. Water molecules are trapped inside the cavities of host oxide network for $n \leq 0.5$. Proton

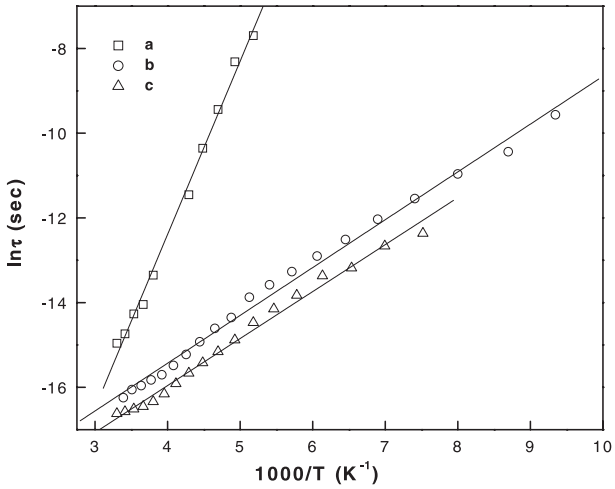

Fig. 10. Temperature variation of relaxation time of (a) $V_2O_5.1.97H_2O$, (b) $(PANI)_{0.64}V_2O_5.0.11H_2O$ (c) $(PANI)_{0.77}V_2O_5.0.06H_2O$.

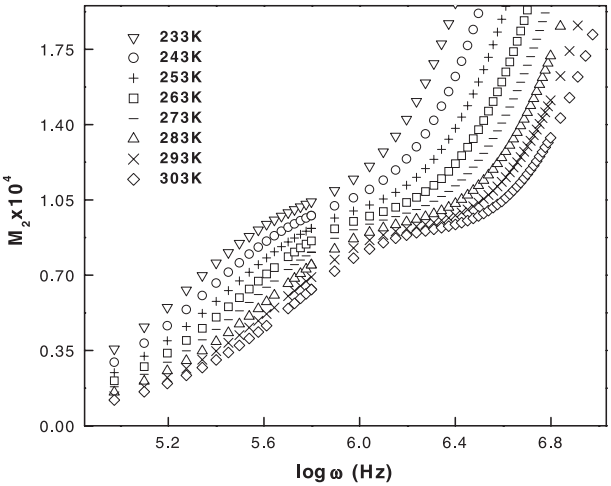

Fig. 11. Imaginary part of electric modulus Vs frequency plot for $(PANI)_{0.77}V_2O_5.0.06H_2O$ at different temperatures.

diffusion between far apart water molecules for low water content is not possible and does not contribute to ionic conduction. Electronic conduction prevails for the intercalated nanocomposites which happens through polaron hopping.

The electric response of various charge carriers is usually interpreted in terms of electric modulus $M = 1/\epsilon$ associated with long range conduction relation. A small contribution in the low frequency region is observed for gel at all temperatures in frequency spectrum of imaginary part, M_2. The frequency dispersion of M_2 for samples S2 and S3 show a part of peak in experimentally available at high frequency region. Isothermal spectra of M_2 are shown in Figure 11 for sample S3. The different formalisms such as complex conductivity, impedance (Z), electric modulus (M) and dielectric permittivity are used to describe different physical processes occurred in the materials [26]. The frequency exponent of real part of conductivity spectra as defined in equation (3) describes the charge

transport mechanism of the system. The complex impedance plots reveal the bulk and interface effects. Studies on dielectric constants provide the dielectric relaxation and its distribution. The small resistance of the bulk leads to very small semicircle relative to interface in complex impedance diagram. The interface effect is suppressed in modulus plot due to high resistance and capacitance of this region of the material. The bulk contribution at higher frequency is magnified in modulus formalism. Thus the various representations obtained from the same experimental data are required to distinguish microscopic processes responsible for dielectric polarization and charge conduction phenomena.

Physical properties of nanocomposites depend on oxide, water and conducting PANI phases. Intercalation of PANI increases V^{+4} ions and decrease water molecule. Nano confinements of PANI within the interlayer space of oxide drastically modify the chain length, conformation and orientation. Moreover interchain interaction is minimized and it is only possible via oxide layers due to the formation of monolayer of PANI. Molecular interaction among PANI, oxide layer and water yield the actual transport properties. The displacements of charge carriers become shorter with the increase of frequency. As a result of it a correlated motion occurs which lead to a strong interaction among the different kinds of charge carriers. The interaction may give significant ac conductivity inspite of very low water content in nanocomposites.

4 Conclusion

Nanocomposites of conducting polyaniline and xerogels are synthesized by redox intercalation technique. Polyaniline of molecular size 5 Å is formed within the interlamellar space of gels. The contribution to dc conductivity is mainly from polyaniline. The complex impedance as a function of temperature shows two semicircles at low and high frequency regions which represent the dominance of bulk and interface effect. Three distinct frequency regions are found in ac conductivity within few MHz regime. The ac conductivity reveals small polaron tunnelling process. The onset and crossover frequencies are thermally activated. The dielectric loss peak frequency is associated with first cross over frequency in ac conductivity. The incorporation of polyaniline into gel induces more Debye like dielectric relaxation process.

This work is funded by the Department of Atomic Energy, Government of India (Project sanction No: 2001/37/4/BRNS). Sukanta De and Ashis Dey are thankful to Council of Scientific and Industrial Research, Government of India for providing fellowship.

References

1. D. O'Hare, in *Inorganic Materials*, edited by D.W. Bruce, D. O'Hare (Wiley, Chichester, 1992), p. 165
2. D.J. Cardin, Adv. Mater. **14**, 553 (2002)
3. M.G. Kanatzidis, C.-G. Wu, H.O. Marcy, C.R. Kannewurf, Adv. Mater. **2**, 364 (1990)
4. S.R. Hwang, W.-H. Li, K.C. Lee, J.W. Lynn, C.-G. Wu, Phys. Rev. B. **62**, 14157 (2000)
5. C.-G. Wu, D.C. DeGroot, H.O. Marcy, J.L. Schindler, C.R. Kannewurf, Y.-J. Liu, W. Hirpo, M.G. Kanatzidis, Chem. Mater. **8**, 1992 (1996)
6. M.G. Kanatzidis, C.-G. Wu, H.O. Marcy, C.R. Kannewurf, J. Am. Chem. Soc. **111**, 4139 (1989)
7. L. Wang, P. Brazis, M. Rocci, C.R. Kannewurf, M.G. Kanatzidis, Chem. Mater. **10**, 3298 (1998)
8. J. Livage, Chem. Mater. **3**, 578 (1991)
9. Y.-J. Liu, J.L. Schindler, D.C. DeGroot, C.R. Kannewurf, W. Hirpo, M.G. Kanatzidis, Chem. Mater. **8**, 525 (1996)
10. Y.-J. Liu, D.C. DeGroot, J.L. Schindler, C.R. Kannewurf, M.G. Kanatzidis, Chem. Mater. **3**, 992 (1991)
11. A. Vadivel Murugan, B.B. Kale, Chai-Won Kwon, G. Campet, K. Vijayamohanan, J. Mater. Chem. **11**, 2470 (2001)
12. J. Lemerle, L. Nejem, J. Lefebvre, J. Inorg. Nucl. chem. **42**, 17 (1980)
13. N.F. Mott, E. Davis, *Electronic Process in Non Crystalline Materials*, 2nd edn. (Oxford, Clarendon, 1979)
14. A.R. Long, Adv. Phys. **31**, 553 (1982)
15. S.R. Elliott, Adv. Phys. **36**, 135 (1987)
16. P. Dutta, S. Biswas, S.K. De, J. Phys.: Condens. Matter **13**, 9187 (2001)
17. D.L. Sidebottom, P.F. Green, R.K. Brow, Phys. Rev. Lett. **74**, 5068 (1995)
18. L.J. Adriaanse, J.A. Reedijk, P.A.A. Teunissen, H.B. Brom, Phys. Rev. Lett. **78**, 1755 (1997)
19. P. Maass, J. Petersen, A. Bunde, W. Dieterich, H.E. Roman, Phys. Rev. Lett. **66**, 52 (1991)
20. T. Ishii, T. Abe, J. Phys. Soc. Jpn **69**, 2549 (2000)
21. T. Ishii, T. Abe, H. Shirai, Solid Stat. Commun. **127**, 737 (2003)
22. J.C. Badot, A. Fourrier-Lamer, N. Baffier, J. Phys. France **46**, 2107 (1985)
23. A.K. Jonscher, *Dielectric Relaxation in solids* (Chesla Dielectrics, London, 1983)
24. J. Livage, Coord. Chem. Rev. **178-180**, 999 (1998)
25. J. Livage, Coord. Chem. Rev. **190-192**, 391 (1999)
26. R. Gerhardt, J. Phys. Chem. Solids **55**, 1491 (1994)